Pressure-induced structural distortion of TbMnO$_3$: A combined x-ray diffraction and x-ray absorption spectroscopy study

J. M. Chen,[1,*] T. L. Chou,[1] J. M. Lee,[1,2] S. A. Chen,[1] T. S. Chan,[1] T. H. Chen,[1] K. T. Lu,[1] W. T. Chuang,[1] H.-S. Sheu,[1]
S. W. Chen,[1] C. M. Lin,[3] N. Hiraoka,[1] H. Ishii,[1] K. D. Tsuei,[1] and T. J. Yang[2]

[1]*National Synchrotron Radiation Research Center (NSRRC), Hsinchu 30076, Taiwan, Republic of China*
[2]*Department of Electrophysics, National Chiao Tung University, Hsinchu 30010, Taiwan, Republic of China*
[3]*Department of Applied Science, National Hsinchu University of Education, Hsinchu 30014, Taiwan, Republic of China*

The variation of electronic states and structural distortion in highly compressed multiferroic TbMnO$_3$ was probed by x-ray diffraction (XRD) and x-ray absorption spectroscopy (XAS) using synchrotron radiation. Refined XRD data enabled observation of a reduced local Jahn-Teller (JT) distortion of Mn sites within MnO$_6$ octahedra in TbMnO$_3$ with increasing hydrostatic pressure. A progressively increasing intensity of the white line in Mn K-edge x-ray absorption spectra of TbMnO$_3$ was detected with increasing pressure. The absorption threshold of Mn K-edge spectra of TbMnO$_3$ is shifted toward higher energy, whereas the pre-edge peak is slightly shifted to lower energy with increasing hydrostatic pressure. We provide spectral evidence for pressure-induced bandwidth broadening for mangnites. The enhanced intensity of the white line and the shifted absorption threshold of Mn K-edge spectra are explained in terms of a reduced JT distortion of MnO$_6$ octahedra in compressed TbMnO$_3$. Comparison of XAS data with full-multiple-scattering calculations using code FDMNES shows satisfactory agreement between experimental and calculated Mn K-edge spectra.

I. INTRODUCTION

Manganese perovskite materials RMnO$_3$ and their derivatives R_xA_{1-x}MnO$_3$, in which R is a trivalent rare-earth element A divalent alkaline-earth element, exhibit many exceptionally interesting phenomena including colossal magnetoresistance (CMR),[1–5] half-metallic behavior,[6,7] strong magnetoelectric coupling,[8–15] and phase separation.[16–20] Magnetoelectric (ME) multiferroics, which exhibit coexisting magnetism and ferroelectricity with cross coupling, are being extensively investigated because of the scientific importance of the electronic origin of magnetoelectrics and relevant prospective applications in devices with new functionalities. The characteristics of magnetoelectric multiferroics include spontaneous magnetization that can be switched with an applied electric field, a spontaneous electrical polarization that can be reoriented with an applied magnetic field via strong magnetoelectric coupling in these materials. The multiferroicity is observed in such manganites as TbMnO$_3$, DyMnO$_3$, and TbMn$_2$O$_5$.[2–5] The quest to understand the origin of multiferroicity has stimulated a great interest in the magnetic, structural, and dielectric properties of multiferroic materials.

At ambient pressure and temperature, TbMnO$_3$ exhibits an orthorhombically distorted perovskite structure with *Pbnm* symmetry containing a network of corner-sharing MnO$_6$ octahedron, as illuminated in Fig. 1. The MnO$_6$ octahedra in TbMnO$_3$ are highly distorted with an average in-plane Mn-O2-Mn bond angle $\sim 145°$ originating from the size mismatch between the Tb^{3+} ion and free space at the center of pseudocubic units.[21] The Jahn-Teller (JT) distortion of the Mn^{3+}O$_6$ octahedra produces three pairs of Mn-O bonds—one Mn-O1 for apical bonds along the c axis, and two Mn-O2 for equatorial bonds in the ab plane. In the basal ab plane, long Mn-O2(l) and short Mn-O2(s) bonds alternate.

TbMnO$_3$ exhibits an incommensurate (IC) lattice modulation at the Néel temperature ($T_N = 42$ K) corresponding to sinusoidal antiferromagnetic (AF) ordering along the b axis. The transition to a noncollinear spiral spin configuration ($T \sim 27$ K) is accompanied with ferroelectric ordering with a polarization $P \| c$.[8] The ME effect is thus closely correlated with the noncollinear spin configurations induced by a significant cooperative Jahn-Teller distortion of MnO$_6$ octahedra and a large octahedra tilt angle.[22] The JT distortion and tilt angle of MnO$_6$ octahedra in TbMnO$_3$ can become modified when smaller ions or divalent cations are incorporated into the rare-earth sites or when a hydrostatic pressure is applied.[21,23] The effect of a hydrostatic pressure on the insulator-metal transitions (IMT) and magnetic states of rare-earth manganites has been observed.[24–29] It was proposed that the variation of electron bandwidth under an external hydrostatic pressure is a driving force in inducing IMT of manganites.[25] However, spectral evidence for pressure-induced bandwidth changes in rare-earth mangnites is still in infancy. The effect of temperature and magnetic field on the orthorhombic *Pbnm* perovskite structure of RMnO$_3$ (R =Gd,Tb,Dy) is well studied,[8–10] but the effect of pressure on highly distorted multiferroic RMnO$_3$ (R=Gd,Tb,Dy) is less well understood.

X-ray diffraction measurements using synchrotron radiation are widely applied for structural investigation of materials under high pressure. Besides the sensitivity to modified electronic structure, the chemical selectivity of x-ray absorption spectroscopy (XAS) provides insight complementary to diffraction measurements in the determination of the local environment around the photoabsorber atom in high-pressure structures of materials. The K-edge absorption spectra of transition-metal oxides reveal a strong dependence on the charge distribution and symmetry distortions of the probed site in materials.[30–33]
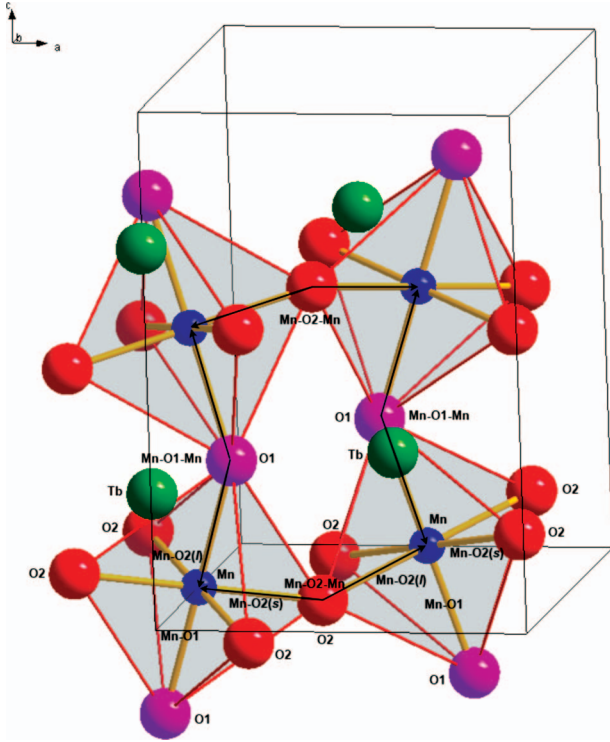
FIG. 1. (Color) Crystal structure of TbMnO$_3$

tering (RIXS)-derived techniques, so-called lifetime broadening suppressed x-ray absorption spectroscopy in the partial fluorescence yield.[34] The high-resolution XAS spectra, particularly in the pre-edge region, provide accurate spectroscopic information on the electronic structure of materials under pressure. Combined with x-ray diffraction, XAS allows one to follow the evolution of the local electronic structure and crystal structure under high pressure. In this work we probed the variation of electronic states and structural distortion in highly compressed multiferroic TbMnO$_3$ with x-ray diffraction and high-resolution x-ray absorption spectra using synchrotron radiation, and we compared the XAS data with full-multiple-scattering calculations using code FDMNES.[35]

II. EXPERIMENTAL

Polycrystalline TbMnO$_3$ was synthesized with a conventional citrate-gel process. Tb$_4$O$_7$ and MnO in a stoichiometric proportion were stirred and dissolved in aqueous solutions of citric and nitric acids. The solution was heated at 85 °C until a spongy gel formed and then heated at a higher temperature to obtain dark-colored ashes. After grinding in a mortar, the dark-colored powder was first calcinated at 600 °C in air to remove organic residues and then further calcinated at 950 °C in air for 12 h. The crystalline structure

However, K-edge XAS resolution is eventually limited by the 1s core-hole lifetime of transition metals of <1.15 eV. In this study, we employed the resonant inelastic x-ray scat-
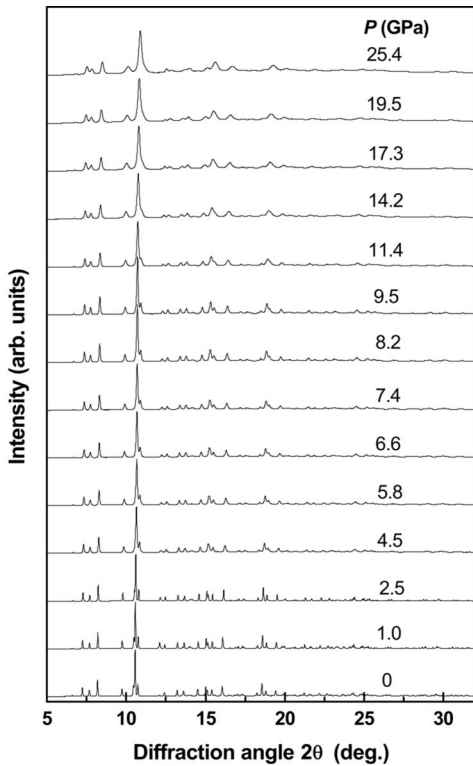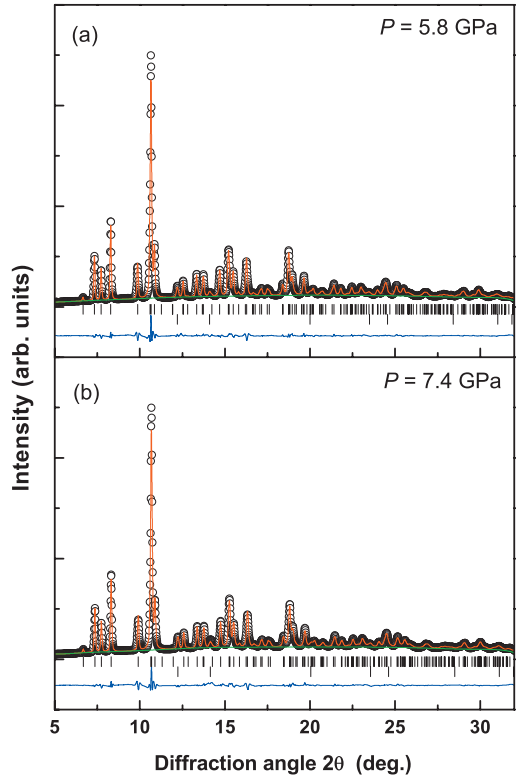

FIG. 2. X-ray diffraction patterns of TbMnO$_3$ for the hydrostatic pressure from ambient to ~26 GPa.

FIG. 3. (Color) X-ray diffraction patterns for TbMnO$_3$ (circles) with their results of Rietveld refinement (red line) and residuals (blue line) for pressures (a) $P=5.8$ GPa and (b) $P=7.4$ GPa. The first row of the vertical marks at an individual pressure corresponds to calculated peak positions of TbMnO$_3$ and the second row to the Au reference as a pressure indicator.

TABLE I. Room-temperature structural parameters for $TbMnO_3$ (*Pbnm*) at four selected pressures.

P (GPa)	0	1.0	5.8	7.4
		Lattice parameters		
a (Å)	5.30601(7)	5.29101(5)	5.24279(17)	5.22645(19)
b (Å)	5.85387(8)	5.83676(6)	5.76514(18)	5.74384(20)
c (Å)	7.41302(10)	7.39636(7)	7.36185(22)	7.34910(25)
Volume	230.353(5)	228.417(8)	222.515(12)	220.619(13)
		Atomic positions		
$Tb(x)$	0.98322(22)	0.98298(19)	0.98140(28)	0.98096(30)
$Tb(y)$	0.08086(13)	0.08088(11)	0.07967(18)	0.07966(20)
$O1(x)$	0.1098(16)	0.1099(14)	0.1185(19)	0.1204(21)
$O1(y)$	0.4674(15)	0.4699(13)	0.4665(21)	0.4723(23)
$O2(x)$	0.7094(14)	0.7107(12)	0.7124(17)	0.7143(19)
$O2(y)$	0.3263(12)	0.3259(11)	0.3152(15)	0.3133(17)
$O2(z)$	0.0506(8)	0.0500(7)	0.0517(10)	0.0503(11)
		Reliability Factors		
$R_p(\%)$	4.21	3.76	3.51	3.48
$R_{wp}(\%)$	5.68	5.00	4.92	4.82
χ^2	0.83	0.68	0.98	1.11

of $TbMnO_3$ was verified with synchrotron x-ray powder diffraction. High-quality orthorhombic $TbMnO_3$ was used for subsequent experiments with elevated pressures.

The pressure-dependent Mn K-edge x-ray absorption measurements were conducted at the Taiwan Beamline BL12XU of SPring-8 in Japan.[36] A fine grained powder sample $TbMnO_3$ was loaded in a 150 μm diameter hole of a Be gasket mounted on a Mao-Bell-type diamond anvil cell (DAC) with 550 μm culet size. Silicone oil was served as a pressure-transmitting medium. The pressure in the cell was measured through the line shift of ruby luminescence with an accuracy ~0.1 GPa. The value averaged over the pressures determined for ruby powder located at various positions on the sample surface was served as the pressure on the sample. The incident beam was monochromatized with two Si(111) crystals and focused to ~16×20 μm at the sample using a pair of 1 m long K-B focusing mirrors. The emitted x-ray fluorescence was then collected at 90° from the incident x rays and analyzed with a Si(440) spherically bent analyzer of a spectrometer (with Rowland circle 1 m radius) arranged on a horizontal plane. The overall resolution, determined from the quasielastic scattering from the sample, was about 0.9 eV full width at half maximum (FWHM). The incident energy was calibrated with the known Mn metal K-edge absorption inflection point at 6539 eV. When the pressure was varied, the detector position was invariably tested with an alignment scan to confirm that the detector was correctly aligned.

The high-pressure x-ray powder diffraction measurements were performed at BL01C2 beamline of the National Synchrotron Radiation Research Center (NSRRC) in Taiwan. An incident x-ray wavelength 0.4959 Å (25 keV), generated from the superconducting wavelength-shifter beamline using a Si(111) double-crystal monochromator, was used for XRD measurements. The as-grown $TbMnO_3$ powder was loaded into the pinhole (diameter 235 μm) of a stainless-steel gasket with Au powder (99.9%, Aldrich) as a pressure indicator.

Methanol-ethanol-water (16:3:1) was served as a pressure-transmitting medium, respectively, in a diamond anvil for XRD measurements. The XRD pattern was recorded with a MAR345 imaging plate for a typical exposure duration ~20 min. The 1D XRD pattern was transformed from 2D diffraction rings using program FIT2D. The diffraction data were structurally refined with the Rietveld method as implemented in software package GSAS (general structure analysis system). An Au powder standard was used to determine precisely the wavelength and the distance from sample to detector.

III. RESULTS AND DISCUSSION

Figure 2 displays representative x-ray diffraction patterns of $TbMnO_3$ over the hydrostatic pressure from ambient to ~26 GPa at room temperature. The gradual increase in the broadening of the x-ray diffraction peaks with pressure is clearly observed in Fig. 2. Line broadening of the x-ray diffraction peaks with increasing hydrostatic pressures is related to the reduction in particle size and enhancement of lattice strains associated with pressure gradients in the samples.[37] Selected x-ray diffraction patterns of $TbMnO_3$ at $P=5.8$ and 7.4 GPa ($T=298$ K) with their corresponding Rietveld refinement are shown in Fig. 3. In the entire range of pressure up to 26 GPa, the crystal structure of $TbMnO_3$ retains its initial *Pbnm* symmetry. Rietveld analysis of the powder diffraction patterns allow us to refine the full crystal structure

up to ∼8 GPa, yielding the lattice parameters and atomic positions. The structural parameters of TbMnO$_3$ calculated from the diffraction data for four selected pressures are given in Table I. Satisfactory agreement between experimental data and their Rietveld refinement is evident from the small values of reliability parameters R_{wp}, R_p, and χ^2 shown in Table I. The values of structural parameters obtained at ambient pressure agree satisfactorily with those in the literature.[21]

To elucidate the pressure-induced structural distortion, we reproduce in Fig. 4(a)–4(c) the pressure dependence of Mn-O distances including the apical Mn-O1 distance and two equatorial Mn-O2 distances, Tb-O distances, and the in-plane Mn-O2-Mn bond angle, respectively. These values are calculated from the structural parameters in Table I. As noted from Fig. 4(a), the short equatorial bond distance Mn-O2(s) and the apical Mn-O1 distance remain virtually unchanged for a hydrostatic pressure less than 8 GPa, the largest effect being a shortening of the long equatorial bond distance Mn-O2(l). The average distances of Tb-O1 and Tb-O2 bonds of the MnO$_6$ octahedra decrease almost linearly with increasing hydrostatic pressure, as shown in Fig. 4(b). The in-plane Mn-O2-Mn tilt angle of two adjacent MnO$_6$ octahedra [i.e., (180°–Mn-O2-Mn bond angle)/2] decreases monotonically with increasing pressure, as deduced from Fig. 4(c). This observation indicates a reduction in the local JT distortion of the Mn site within MnO$_6$ octahedra with increasing hydrostatic pressure.

Figure 5 shows Mn K-edge high-resolution XAS spectra of polycrystalline TbMnO$_3$ collected at various pressures up to ∼30 GPa. The spectra were obtained in partial fluorescence yield, with the spectrometer energy fixed at the maximum of the Mn $K\beta_{1,3}$ line. The Mn K-edge XAS spectra of TbMnO$_3$ consist of two well resolved peaks in the pre-edge region (labeled P1 and P2) and an intense white line at the side of higher photon energy (labeled B in Fig. 5). Based on the polarized $1s3p$-resonant x-ray emission spectra (RXES) at the Mn K edge of TbMnO$_3$ single crystals along the three crystallographic directions, unoccupied Mn $3d$ states exhibit a relatively delocalized character as a result of hybridization of unoccupied Mn $3d$ states with neighboring Mn $4p$ orbitals.[38]

To ensure a proper assignment of the pre-edge features labeled P1 and P2 in Fig. 5, we performed band-structure calculations in a local-density approximation plus on-site Coulomb interaction U (LDA+U) for hypothetical A-type AF, E-type AF, and ferromagnetic (FM) structures of TbMnO$_3$. The band-structure calculations were performed using the full-potential projected augmented wave method as implemented in the Vienna *ab initio* simulation package (VASP) within the local-density approximation plus on-site Coulomb interaction U (LDA+U) scheme. In the LDA+U calculations, Coulomb energy U=5.0 eV and exchange parameter J=0.87 eV for Mn-$3d$ electrons were used.[39] Fig. 6 displays the partial density of states of Mn projected onto the fivefold $3d$ orbitals. Mn $3d$ bands split into the low-lying t_{2g} (d_{xy}, d_{yz}, and d_{zx}) and high-lying e_g orbitals. Through a strong JT effect, the $e_g\uparrow$ band splits into two subbands $e_g^1\uparrow$ and $e_g^2\uparrow$ in TbMnO$_3$. There is a small indirect gap between the JT-split Mn $e_g^1\uparrow$ and $e_g^2\uparrow$ bands, in agreement with the experimental observation of an insulating behavior of

TbMnO$_3$. P1 in Fig. 5 is ascribed to transitions of Mn $1s$ core electrons into unoccupied majority-spin Mn $e_g\uparrow$ states hybridized with the neighboring Mn $4p$ states. P2 in Fig. 5 is assigned as a superposition of transitions into empty minority-spin $t_{2g}\downarrow$ and $e_g\downarrow$ states hybridized with the neighboring $4p$ states. The white line (labeled B in Fig. 5) is attributed to transitions from Mn $1s$ to Mn $4p$. Feature C in Fig. 5 results from the multiple-scattering contribution of MnO$_6$ surrounded by eight Tb.

As shown in Fig. 5, the Mn K-edge XAS spectra of TbMnO$_3$ collected at varied pressures exhibit slight modifications, indicating that the local atomic manganese environment of TbMnO$_3$ is not much altered under an external hydrostatic pressure up to ∼30 GPa, consistent with present XRD results. As noted, the intensity of white line labeled B (6555–6565 eV) in Mn K-edge x-ray absorption spectra of TbMnO$_3$ increases progressively with increasing external hydrostatic pressure. Besides, the absorption threshold and peak C of Mn K-edge spectra of TbMnO$_3$ gradually shift toward higher energy, whereas the pre-edge peak labeled P1 continuously shifts to lower energy as a hydrostatic pressure increases. The pre-edge peak of Mn K-edge x-ray absorption spectrum of TbMnO$_3$ at P=30 GPa is shifted to lower energy ∼0.3 eV as compared with that at P=1 GPa.

Based on the LDA+U calculations, the occupied $e_g^1\uparrow$ and unoccupied $e_g^2\uparrow$ bands are dominated by $d_{3x^2-r^2}$ and $d_{y^2-z^2}$ orbitals, respectively, in one coplanar Mn ion, whereas they exhibit predominantly $d_{3y^2-r^2}$ and $d_{x^2-z^2}$ character, respectively, for the other coplanar Mn ion.[39] TbMnO$_3$ hence exhibits a staggered $d_{3x^2-r^2}/d_{3y^2-r^2}$-type orbital ordering in the ab plane, similar to that of YMnO$_3$ and LaMnO$_3$.[40,41] The half-filled $e_g^1\uparrow$ orbitals of Mn^{3+} ions occupy the long Mn-O2(l) site projected predominantly along the b axis, whereas unoccupied $e_g^2\uparrow$ orbitals locate at the short Mn-O2(s) site projected predominantly along the a axis. Alternating long Mn-O2(l) and short Mn-O2(s) distances in the ab plane of the structure in TbMnO$_3$ are a precursor of orbital ordering. The splitting of the $e_g\uparrow$ orbitals in the $t_{2g}^3 e_g^1$ electron configuration of the Mn^{3+} ions is therefore closely related to the JT distortion and the orbital ordering within the
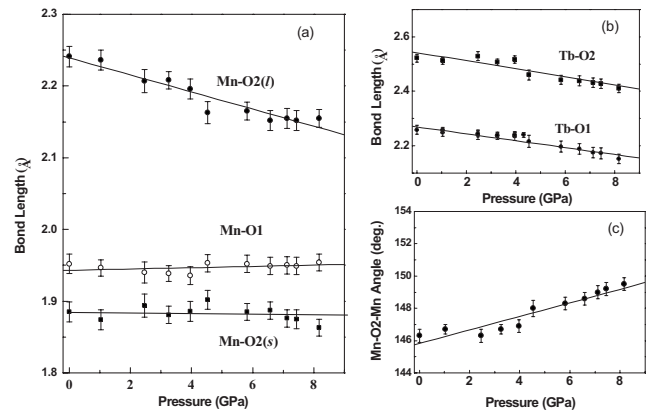

FIG. 4. Pressure dependence of (a) Mn-O distances including apical Mn-O1 distance and two equatorial Mn-O2 equatorial distances, (b) Tb-O distances, and (c) Mn-O2-Mn bond angle of distorted MnO$_6$ octahedra in TbMnO$_3$.
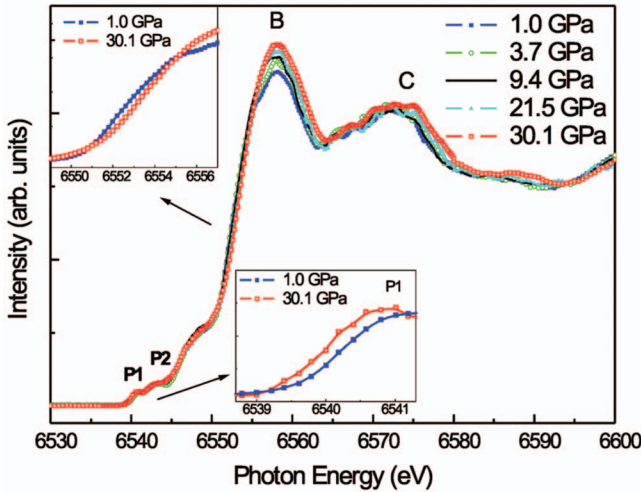
FIG. 5. (Color) Mn K-edge high-resolution XAS spectra, collected by the partial fluorescence yield, of polycrystalline TbMnO$_3$ at various pressures up to ~30 GPa. The insets show an enlarged pre-edge region and near the threshold.

MnO$_6$ octahedra in TbMnO$_3$. The highly distorted MnO$_6$ octahedra and orbital ordering in TbMnO$_3$ leads to the highly anisotropic Mn-O bonding within the ab plane, and in turn to the frustrated magnetic ordering caused by the competitions of the ferromagnetc nearest-neighbor (NN) superexchange interaction and the antiferromagnetc diagonal next-nearest-neighbor (NNN) superexchange interaction in b direction, in particular spiral spin structures, responsible for their multiferroic behavior in TbMnO$_3$.[22]

As shown in Fig. 4, the pressure effect is most pronounced for the long equatorial distance Mn-O2(l) that relates to the larger compressibility along the b axis under pressure. The compressive anisotropy of MnO$_6$ octahedra
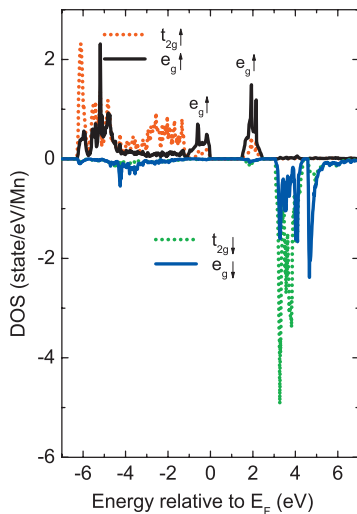

FIG. 6. (Color) Partial densities of states of Mn projected onto fivefold 3d orbitals for a hypothetical A-type antiferromagnetic structure of TbMnO$_3$ calculated with the LDA+U method. The parameters in these calculations are described in the text. For each panel the upper half denotes the majority and the lower half the minority-spin states. The energy zero is at the Fermi energy (E_f).
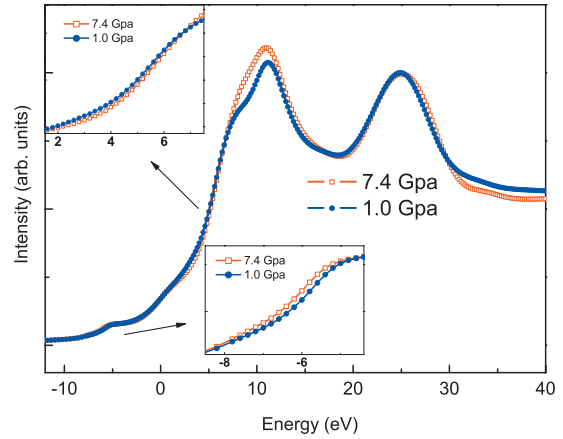

FIG. 7. (Color) Mn K-edge XAS spectra of TbMnO$_3$ with varied hydrostatic pressures simulated using code FDMNES for cluster radius $R=5$ Å. The insets show an enlarged pre-edge region and near the threshold.

with hydrostatic pressure in TbMnO$_3$ should lead to redistribution of the density of states. The electronic bandwidth of $e_g\uparrow$ orbitals is a particularly important parameter for determining the complicated properties of manganites, such as the bandwidth-driven transition from insulator to metal.[25,42] The bandwidth of the $e_g\uparrow$ orbitals in maganites is characterized by the overlap between the Mn 3d and O 2p orbitals and is highly correlated with the local atomic structure of MnO$_6$ octahedra including the equatorial Mn-O2 distances and the in-plane Mn-O2-Mn tilt angle.[43] As confirmed by the present XRD measurements, an observed decrease in equatorial Mn-O2 distances and the decreasing octahedral Mn-O2-Mn tilt angle under hydrostatic pressure both enhance the hybridization of the Mn 3d and O 2p orbitals and hence broaden the electronic bandwidth of the $e_g\uparrow$ orbitals in TbMnO$_3$.[43] The unoccupied $e_g\uparrow$ state is expected to be shifted toward the Fermi level, mediated by increased electronic bandwidth of $e_g\uparrow$ orbitals in TbMnO$_3$ under an external pressure.[25,42] The pre-edge peak P1 originating from transitions of Mn 1s core electrons to unoccupied Mn 3$d(e_g\uparrow)$ states is accordingly gradually shifted toward lower energy when a hydrostatic pressure is applied, as evident in Fig. 5.

The polarization-dependent Mn K-edge x-ray absorption spectra of TbMnO$_3$ single crystals exhibit a significant anisotropy along the three crystallographic directions $E\|a$, $E\|b$, and $E\|c$, particularly for the white-line region.[38] A significant energy shift to lower energy ~2.4 eV is observed for the maximum of the white line of the Mn K-edge spectrum obtained along $E\|b$ relative to $E\|a$ and E$\|c$, indicating a highly anisotropic Mn-O bonding within the ab plane in TbMnO$_3$ and relatively weak covalency along the b axis, as supported by present XRD results. The origin of this energy difference is attributed to the JT distortion and orbital ordering of MnO$_6$ octahedra in TbMnO$_3$.[44] When the long equatorial bond distance Mn-O2(l) projected predominantly along the b axis is greatly decreased with increasing hydrostatic pressure and becomes nearer the short equatorial bond length Mn-O2(s) projected predominantly along the a axis, as evident in Fig. 4(a), the absorption edge of Mn K-edge spectrum for E$\|b$ of TbMnO$_3$ gradually shifts to higher en-

ergy. The separation for the maximum of the white line of the Mn K-edge spectra between E‖b and E‖a of TbMnO$_3$ becomes smaller due to a reduced JT distortion of TbMnO$_3$ under an external hydrostatic pressure. An increased overlap between the $E‖b$ spectrum and the $E‖a$ spectrum under pressure consequently generates an increased white-line intensity of Mn K-edge spectra of polycrystalline TbMnO$_3$.[45]

Based on the structural parameters at various pressures in Table I, the Mn K-edge XAS calculations of TbMnO$_3$ were performed by the FDMNES code.[35] In the present XAS simulation, muffin-tin (MT) full-multiple-scattering (FMS) approach was applied with a cluster radius $R=5$ Å. The FMS calculations were performed using the MT potential constructed from 10% overlapped MT spheres of the radii. Figure 7 shows simulated Mn K-edge XAS spectra of TbMnO$_3$ with varied hydrostatic pressures. An increase in the white-line intensity with increasing pressure is clearly observed. As shown in insets of Fig. 7, the absorption threshold of simulated Mn K-edge spectra of TbMnO$_3$ is shifted toward higher energy, whereas the pre-edge peak becomes shifted to lower energy with increasing pressure. The experimental and calculated Mn K-edge spectra agree satisfactorily.

IV. CONCLUSION

The variation of electronic states and structural distortion in highly compressed multiferroic TbMnO$_3$ were probed by combining the measurements of synchrotron x-ray powder diffraction and high-resolution x-ray absorption spectroscopy in the partial fluorescence yield. The Jahn-Teller distortion and orbital ordering within the MnO$_6$ octahedra in orthorhombic TbMnO$_3$ produce a long equatorial bond Mn-O2(l) and a short equatorial bond Mn-O2(s) in the basal ab plane. The short equatorial bond distance Mn-O2(s) and the apical Mn-O1 distance remain virtually unchanged for a hydrostatic pressure less than 8 GPa, the largest effect being a shortening of the long equatorial bond distance Mn-O2(l). The in-plane Mn-O2-Mn tilt angle of two adjacent MnO$_6$ octahedra decreases monotonically with increasing pressure. Based on these XRD results, a decreased local JT distortion of Mn sites within MnO$_6$ octahedra in TbMnO$_3$ was observed with increasing hydrostatic pressure. The intensity of the white line in Mn K-edge x-ray absorption spectra of TbMnO$_3$ increases progressively with increasing pressure. The absorption threshold of Mn K-edge spectra of TbMnO$_3$ shifted toward higher energy, whereas the pre-edge peak slightly shifted to lower energy with increasing hydrostatic pressure. We provide spectral evidence for pressure-induced bandwidth broadening for mangnites. The enhanced intensity of the white line and the shift of the absorption threshold of Mn K-edge spectra are attributed to the reduced Jahn-Teller distortion of MnO$_6$ octahedra in TbMnO$_3$ when a hydrostatic pressure is applied. Comparison of XAS data with full-multiple-scattering calculations using code FDMNES shows satisfactory agreement between experimental and calculated Mn K-edge spectra.

*Author to whom correspondence should be addressed.

[1] E. Dagotto, T. Hotta, and A. Moreo, Phys. Rep. **344**, 1 (2001).

[2] *Colossal Magnetoresistance Oxides*, edited by Y. Tokura (Gordon and Breach, New York, 2000).

[3] S. Jin, T. H. Tiefel, M. McCormack, R. A. Fastnacht, R. Ramesh, and L. H. Chen, Science **264**, 413 (1994).

[4] R. von Helmolt, J. Wecker, B. Holzapfel, L. Schultz, and K. Samwer, Phys. Rev. Lett. **71**, 2331 (1993).

[5] K. Tokura, A. Urushibara, Y. Moritomo, T. Arima, A. Asamitsu, G. Kido, and N. Furukawa, J. Phys. Soc. Jpn. **63**, 3931 (1994).

[6] W. E. Pickett and D. J. Singh, Phys. Rev. B **53**, 1146 (1996).

[7] M. S. Laad, L. Craco, and E. Müller-Hartmann, New J. Phys. **6**, 157 (2004).

[8] T. Kimura, T. Goto, H. Shintani, K. Ishizaka, T. Arima, and Y. Tokura, Nature (London) **426**, 55 (2003).

[9] N. Hur, S. Park, P. A. Sharma, J. S. Ahn, S. Guha, and S-W. Cheong, Nature (London) **429**, 392 (2004).

[10] T. Goto, T. Kimura, G. Lawes, A. P. Ramirez, and Y. Tokura, Phys. Rev. Lett. **92**, 257201 (2004).

[11] N. A. Spaldin and M. Fiebig, Science **309**, 391 (2005).

[12] W. Eerenstein, N. D. Mathur, and J. F. Scott, Nature (London) **442**, 759 (2006).

[13] R. Ramesh and N. A. Spaldin, Nature Mater. **6**, 21 (2007).

[14] L. C. Chapon, G. R. Blake, M. J. Gutmann, S. Park, N. Hur, P. G. Radaelli, and S.-W. Cheong, Phys. Rev. Lett. **93**, 177402 (2004).

[15] M. Fiebig, J. Phys. D **38**, R123 (2005).

[16] M. Fäth, S. Freisen, A. A. Menovsky, Y. Tomioka, J. Aart, and J. A. Mydosh, Science **285**, 1540 (1999).

[17] P. Levy, F. Parisi, L. Granja, E. Indelicato, and G. Polla, Phys. Rev. Lett. **89**, 137001 (2002).

[18] C. Simon, S. Mercone, N. Guiblin, C. Martin, A. Brulet, and G. Andre, Phys. Rev. Lett. **89**, 207202 (2002).

[19] M. Mayr, A. Moreo, J. A. Verges, J. Arispe, A. Feiguin, and E. Dagotto, Phys. Rev. Lett. **86**, 135 (2001).

[20] M. B. Salamon and M. Jaime, Rev. Mod. Phys. **73**, 583 (2001).

[21] J. Blasco, C. Ritter, J. García, J. M. de Teresa, J. Pérez-Cacho, and M. R. Ibarra, Phys. Rev. B **62**, 5609 (2000).

[22] T. Kimura, S. Ishihara, H. Shintani, T. Arima, K. T. Takahashi, K. Ishizaka, and Y. Tokura, Phys. Rev. B **68**, 060403(R) (2003).

[23] C. C. Yang, M. K. Chung, W.-H. Li, T. S. Chan, R. S. Liu, Y. H. Lien, C. Y. Huang, Y. Y. Chan, Y. D. Yao, and J. W. Lynn, Phys. Rev. B **74**, 094409 (2006).

[24] J. J. Neumeier, M. F. Hundley, J. D. Thompson, and R. H. Heffner, Phys. Rev. B **52**, R7006 (1995).

[25] A. Yamasaki, M. Feldbacher, Y.-F. Yang, O. K. Andersen, and K. Held, Phys. Rev. Lett. **96**, 166401 (2006).

[26] H. Y. Hwang, T. T. M. Palstra, S. W. Cheong, and B. Batlogg,

Phys. Rev. B **52**, 15046 (1995).

[27] V. Laukhin, J. Fontcuberta, J. L. Garcia-Munoz, and X. Obradors, Phys. Rev. B **56**, R10009 (1997).

[28] R. Senis, V. Laukhin, B. Martínez, J. Fontcuberta, X. Obradors, A. A. Arsenov, and Y. M. Mukovskii, Phys. Rev. B **57**, 14680 (1998).

[29] A. Nossov, J. Pierre, and J. Beille, V. Vassiliev, and B. Slobodin, Eur. Phys. J. B **6**, 467 (1998).

[30] R. V. Vedrinskii, V. L. Kraizman, A. A. Novakovich, Ph. V. Demekhin, and S. V. Urazhdin, J. Phys.: Condens. Matter **10**, 9561 (1998).

[31] F. Bridges, C. H. Booth, M. Anderson, G. H. Kwei, J. J. Neumeier, J. Snyder, J. Mitchell, J. S. Gardner, and E. Brosha, Phys. Rev. B **63**, 214405 (2001).

[32] A. Yu. Ignatov, N. Ali, and S. Khalid, Phys. Rev. B **64**, 014413 (2001).

[33] T. Shibata, B. A. Bunker, and J. F. Mitchell, Phys. Rev. B **68**, 024103 (2003).

[34] J.-P. Rueff, L. Journel, P.-E. Petit, and F. Farges, Phys. Rev. B **69**, 235107 (2004).

[35] Y. Joly, Phys. Rev. B **63**, 125120 (2001).

[36] Y. Q. Cai, P. Chow, C. C. Chen, H. Ishii, K. L. Tsang, C. C. Kao, K. S. Liang, and C. T. Chen, in *Optical Design and Performance of the Taiwan Inelastic X-ray Scattering Beamline*, edited by T.

Warwick, J. Arthur, H. A. Padmore, and J. Stöhr, AIP Conf. Proc. No. 705 (AIP, New York, 2004), p. 340.

[37] Z. Wang, Y. Zhao, D. Schiferl, C. S. Zha, and R. T. Downs, Appl. Phys. Lett. **85**, 124 (2004).

[38] J. M. Chen, C. K. Chen, T. L. Chou, I. Jarrige, H. Ishii, K. T. Lu, Y. Q. Cai, K. S. Ling, J. M. Lee, S. W. Huang, T. J. Yang, C. C. Shen, R. S. Liu, J. Y. Lin, H. T. Jeng, and C. C. Kao, Appl. Phys. Lett. **91**, 054108 (2007).

[39] J. M. Chen, J. M. Lee, C. K. Chen, T. L. Chou, K. T. Lu, S. C. Haw, K. S. Liang, C. T. Chen, H. T. Jeng, S. W. Huang, T. J. Yang, C. C. Shen, R. S. Liu, J. Y. Lin, and Z. Hu, Appl. Phys. Lett. **94**, 044105 (2009).

[40] S. Picozzi, K. Yamauchi, G. Bihlmayer, and S. Blügel, Phys. Rev. B **74**, 094402 (2006).

[41] I. Solovyev, N. Hamada, and K. Terakura, Phys. Rev. Lett. **76**, 4825 (1996).

[42] I. Loa, P. Adler, A. Grzechnik, K. Syassen, U. Schwarz, M. Hanfland, G. Kh. Rozenberg, P. Gorodetsky, and M. P. Pasternak, Phys. Rev. Lett. **87**, 125501 (2001).

[43] C. Cui and T. A. Tyson, Appl. Phys. Lett. **84**, 942 (2004).

[44] I. S. Elfimov, V. I. Anisimov, and G. A. Sawatzky, Phys. Rev. Lett. **82**, 4264 (1999).

[45] A. Y. Ramos, H. C. N. Tolentino, N. M. Souza-Neto, J. P. Itie, L. Morales, and A. Caneiro, Phys. Rev. B **75**, 052103 (2007).